Sci. Rep. RITU A43 (1997) pp. 195-202
No. 2, March 1997

Structure and Effective Pair Potentials of Molten CuBr Estimated from the Anomalous X-ray Scattering Measurements*

Yoshio Waseda, Masatoshi Saito, Changyong Park and Kazuhiko Omote#

Institute for Advanced Materials Processing, Tohoku University, Sendai 980-77, Japan

(Received January 16,1997)

The anomalous x-ray scattering (AXS) measurements for molten CuBr have been made using the energies close to the Cu K(8.980 keV) and Br K (13.470 keV) absorption edges for estimating three partial structural functions, Cu-Cu, Br-Br and Cu-Br pairs by combining with the intensity data obtained at the energy of 17.0 keV, which is far from both edges. The data processing for obtaining three partials includes the help of the reverse Monte Carlo (RMC) simulation technique. The resultant structure factor of $a_{CuCu}(Q)$ for cation-cation pairs was found to be rather structureless and the closest Cu-Cu distance in molten CuBr was significantly smaller than that of $a_{BrBr}(Q)$ for anion-anion pairs, suggesting the like-ion penetration into the first unlike-ion coordination shell, similar to the molten CuCl case. The effective pair potentials of molten CuBr were also estimated from these experimental partial structural data by applying the modified hypernetted-chain (MHNC) equation coupled with a "predictor-corrector method" originally proposed by Reatto et al. in 1986 for a single component liquid system. It may be worth mentioning that the resultant pair potential for Cu-Cu pairs shows remarkable shielding for the Coulomb repulsion in its nearest neighbor region.

KEYWORDS: anomalous X-ray scattering, partial structure factor, effective pair potential, molten CuBr, reverse Monte Carlo simulation, modified hypernetted-chain equation

1. Introduction

Quantitative description of the atomic scale structure of non-crystalline systems usually employs the radial distribution function (RDF) indicating the probability of finding another atom from an origin atom as a function of radial distance obtained by spherical averaging[1]. The RDF is only one-dimensional but it does give almost unique quantitative information describing the atomic arrangements in non-crystalline systems. On the other hand, surrounding of each atom in multi-component non-crystalline systems generally differs from those of other atoms. This makes the interpretation of their RDFs not so easy. In this respect, the partial RDFs for the individual chemical constituents are of particular importance and the essential items for discussing the structure and properties of multi-component non-crystalline systems at a microscopic level. Then, when the full set of the partial structural functions are obtained, we enables us to understand the relationships between the atomic scale structure and their characteristic properties in a more realistic way. Thus, the determination of partial structural functions is one of the most important subjects for non-crystalline systems such as liquids and glasses including more than two components[2)3)].

The partial structure factors, corresponding to the Fourier transform of RDFs, for a binary system can be estimated only by making available at least three independent intensity measurements for which the weighting factors are varied without any change in their atomic distribution. This has been achieved in neutron diffraction experiments by the isotopic substitution technique, firstly applied by Enderby et al.[4] to liquid Cu-Sn alloys and to several molten salts, as exemplified by Page and Mika's results of CuCl[5]. This neutron method involves scattering from three samples prepared with different isotopic concentrations of the components, that is with different mean neutron scattering lengths. The isotope substitution neutron diffraction method is undoubtedly powerful technique and works well. However, it seems intrinsically to be somewhat limited in practice by availability of suitable isotopes and the structure is automatically assumed to remain identical upon substitution by the isotopes. On the other hand, the anomalous X-ray scattering (hereafter referred to as AXS) method[6)7)] by utilizing the so-called anomalous dispersion effect near the absorption edge of the constitutenet elements appears to provide answers without any assumption for many more elements in the periodic table. The availability of the intense white X-rays from a synchrotron radiation source has greatly improved both acquisition and quality of the AXS data by enabling the use of an energy in which the AXS is the greatest[7].

The main purpose of this work is to report the three partial structural functions of molten CuBr estimated from AXS measurements. The three effective pair potentials will also be calculated from these experimental partial structural data using the modified hypernetted-chain (MHNC) equation[8] along the way similar to the Johnson-March scheme[9].

---

* The 97-R9 report of Institute for Advanced Materials Processing (AMP).

Present Address : X-ray Diffraction Laboratory, Rigaku Co. Ltd.

2. Fundamentals for the AXS analysis and measurements

The method of analyzing the measured AXS intensity data for non-crystalline systems has been discussed previously[7)10)]. For convenience of discussion, only some essential points and additional details which are necessary for the present work are given below.

The partial structure factor of α-β pair, $a_{\alpha\beta}(Q)$, in the Faber-Ziman's form[2)] is connected with the partial pair distribution function $g_{\alpha\beta}(r)$ by the Fourier transformation as follows;

$$a_{\alpha\beta}(Q) = 1 + \frac{4\pi\rho_0}{Q}\int_0^\infty r[g_{\alpha\beta}(r)-1]\sin(Qr)dr, \qquad (1)$$

where ρ_0 is the average number density in the system. On the other hand, the so-called reduced interference function, $i(Q,E)$ for a binary system can be described by the following form using the coherent X-ray scattering intensity $I(Q,E)$ corresponding to the structurally sensitive part of the total scattering intensity;

$$\begin{aligned} i(Q,E) &\equiv I(Q,E) - \sum_\alpha c_\alpha f_\alpha^2(Q,E) \\ &= \sum_{\alpha=1}^{2}\sum_{\beta=1}^{2} c_\alpha c_\beta f_\alpha(Q,E) f_\beta(Q,E)\{a_{\alpha\beta}(Q)-1\} \end{aligned} \qquad (2)$$

where Q and E are the wave vector and the incident X-ray energy, respectively, c_α is the atomic fraction, $f_\alpha(Q,E)$ is the atomic scattering factor of α component. The coefficients of $\{a_{\alpha\beta}(Q)-1\}$ in eq.(2) depend on the concentrations and the atomic scattering factors. Thus, the individual partial structure factors can be estimated from, at least, three independent scattering experiments for which the coefficients are altered. The utilization of anomalous dispersion effect is one way to vary the atomic scattering factors in these coefficients, because a distinct energy dependence due to the anomalous dispersion effect clearly appears in the close vicinity of the absorption edge relevant to K- or L-shell electrons of a constituent. In such energy region, the atomic scattering factor can be expressed by,

$$f(Q,E) = f^0(Q) + f'(E) + if''(E), \qquad (3)$$

where $f^0(Q)$ corresponds to the scattering factor of the atom at the energy sufficiently away from the absorption edge, and $f'(E)$ and $f''(E)$ are the real and imaginary parts of the anomalous dispersion terms. Figure 1 shows the anomalous dispersion terms of isolated Cu and Br atoms in the energy range including the Cu K and Br K absorption edges, which are theoretically calculated with relativistic Cromer-Liberman scheme[11)]. It may be worth mentioning that the value of $f'(E)$ shows a drastic change at the lower energy side of the absorption edge, whereas the value of $f''(E)$ and its energy-variation is quite small in this energy region.

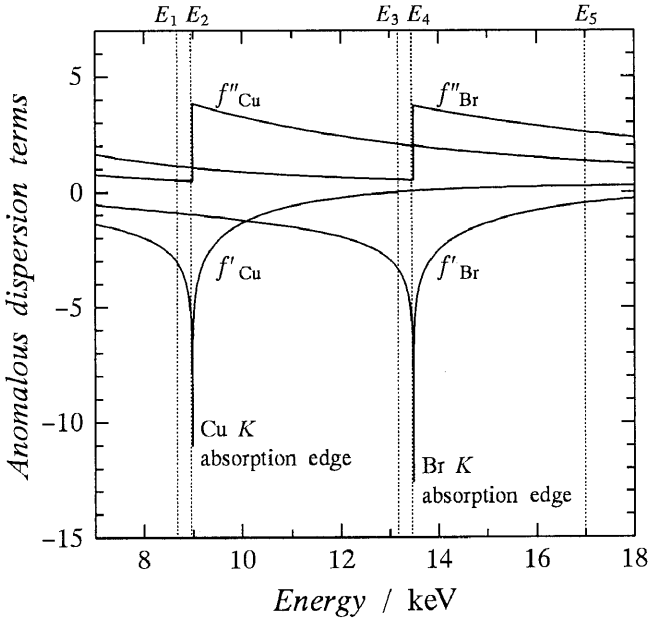

Fig. 1 Energy variations of anomalous dispersion factors for isolated Cu and Br near the K absorption edge, as calculated by the relativistic Cromer and Liberman method[7)11)].

When the incident energy is set to the lower energy side of the absorption edge E_{abs} of a specific element, for example Cu in this case, the anomalous dispersion phenomena becomes significant, and thereby the variation between intensities, $\Delta i_{Cu}(Q,E_1,E_2)$, measured at the incident energies of E_1 and E_2 is attributed to a change in the real part of anomalous dispersion terms of Cu. Therefore, the following relation can readily be obtained.

$$\begin{aligned} \Delta i_{Cu}(Q,E_1,E_2) &\equiv \frac{\{I(Q,E_1)-\langle f^2(Q,E_1)\rangle\}-\{I(Q,E_2)-\langle f^2(Q,E_2)\rangle\}}{c_{Cu}\{f'_{Cu}(E_1)-f'_{Cu}(E_2)\}W(Q,E_1,E_2)} \\ &= \frac{c_{Cu}\Re\{f_{Cu}(Q,E_1)+f_{Cu}(Q,E_2)\}}{W(Q,E_1,E_2)}(a_{CuCu}(Q)-1) \\ &\quad + \frac{c_{Br}\Re\{f_{Br}(Q,E_1)+f_{Br}(Q,E_2)\}}{W(Q,E_1,E_2)}(a_{CuBr}(Q)-1) \end{aligned} \qquad (4)$$

in which

$$W(Q,E_1,E_2) = \sum_{k=1}^{2} c_k \Re\{f_k(Q,E_1)+f_k(Q,E_2)\}, \qquad (5)$$

where $E_{abs}>E_2>E_1$ and $\Re$ denotes the real part of the values in the brackets. The quantity of $\Delta i_{Cu}(Q,E_1,E_2)$ associated with Cu contains two partial structure factors, $a_{CuCu}(Q)$ and $a_{CuBr}(Q)$. Similarly, $\Delta i_{Br}(Q,E_1,E_2)$ measured at the lower energy side of Br K absorption edge contains $a_{BrBr}(Q)$ and $a_{CuBr}(Q)$. Then, in order to obtain the three partial structure factors, the following set of equations should be solved;

$$\begin{pmatrix} \Delta i_{Cu}(Q,E_1,E_2) \\ \Delta i_{Br}(Q,E_3,E_4) \\ i(Q,E_5) \end{pmatrix} = \begin{pmatrix} \frac{c_{Cu}\Re\{f_{Cu}(Q,E_1)+f_{Cu}(Q,E_2)\}}{W(Q,E_1,E_2)} & \frac{c_{Br}\Re\{f_{Br}(Q,E_1)+f_{Br}(Q,E_2)\}}{W(Q,E_1,E_2)} & 0 \\ 0 & \frac{c_{Cu}\Re\{f_{Cu}(Q,E_3)+f_{Cu}(Q,E_4)\}}{W(Q,E_3,E_4)} & \frac{c_{Br}\Re\{f_{Br}(Q,E_3)+f_{Br}(Q,E_4)\}}{W(Q,E_3,E_4)} \\ c_{Cu}^2 f_{Cu}^2(Q,E_5) & 2c_{Cu}c_{Br}f_{Cu}(Q,E_5)f_{Br}(Q,E_5) & c_{Br}^2 f_{Br}^2(Q,E_5) \end{pmatrix} \begin{pmatrix} a_{CuCu}(Q)-1 \\ a_{CuBr}(Q)-1 \\ a_{BrBr}(Q)-1 \end{pmatrix}. \qquad (6)$$

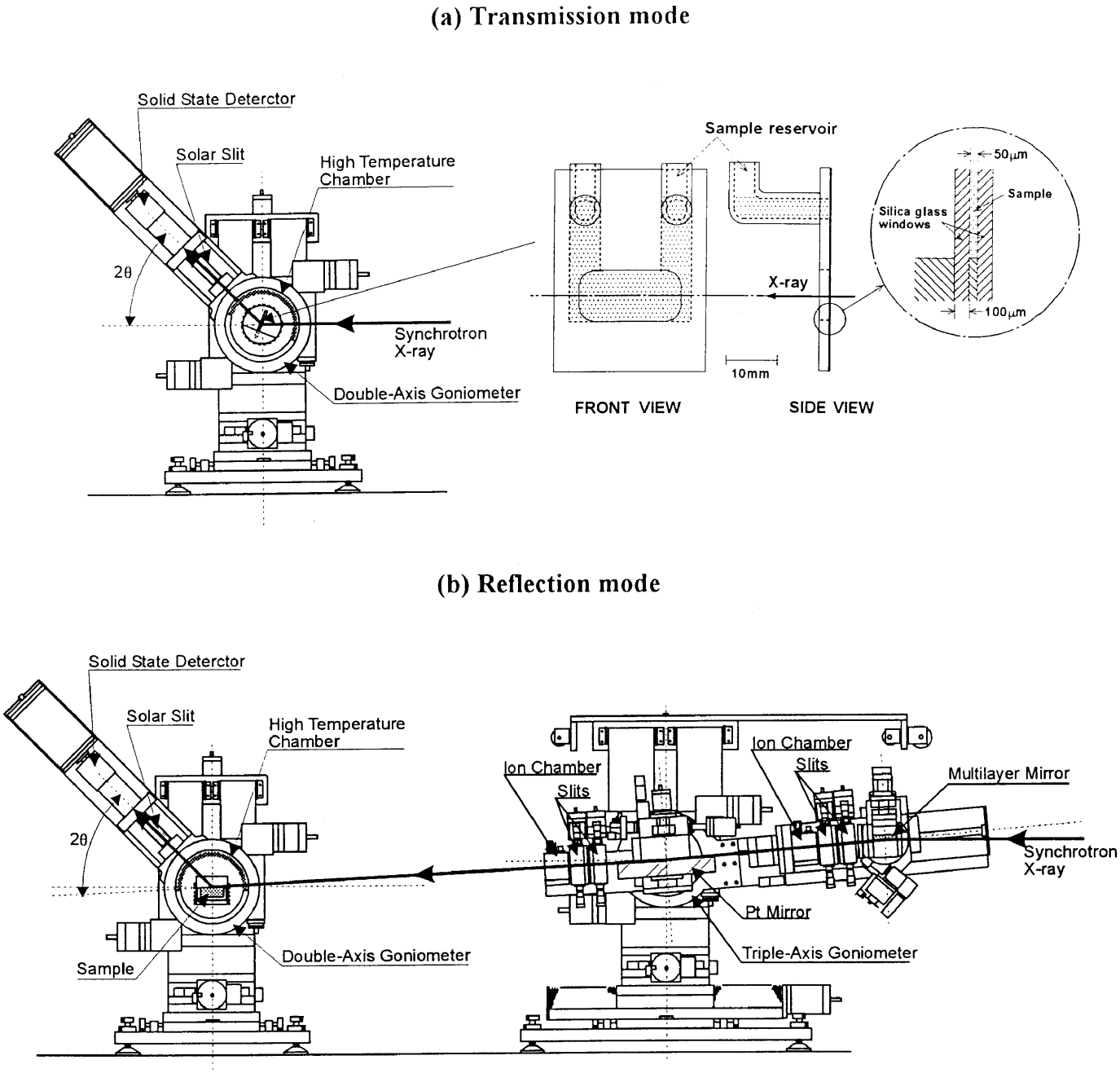

Fig. 2 Schematic diagram of the AXS measurements for liquid samples made in (a) the transmission mode with a devised quartz cell and (b) the reflection mode from a free surface by changing the beam direction using an additional multi-layers mirror system.

The AXS measurements for molten CuBr sample were carried out with synchrotron radiation at a beam line (6B and 7C station) where a Si(111) double-crystal monochromator covering the energies ranging from 4 to 21 keV is available in the Photon Factory of the National Laboratory for High-Energy Physics, Tsukuba, Japan. Details of the experimental setting have already been reported[12] and not duplicated here. It may be noteworthy that the AXS measurements can be made in both transmission mode with a devised quartz cell (a sample space of the order of 50 μ m) and reflection mode from a free surface by changing the beam direction using an additional multi-layers mirror system. For convenience, these two settings are shown in Fig. 2.

The incident beam was monitored by a N_2 gas flow type ion chamber placed in front of the sample so as to keep constant the number of photons incident on the sample. The scattering intensities were measured by a Si(Li) solid state detector so that the fluorescent radiation from the sample in the measurement near the absorption edge can be removed from the elastic scattering with a pulse height analyzer. The anomalous dispersion terms for Cu and Br for energies measured in this work are listed in Table 1. The normal atomic scattering factors are taken from the compilation of *International Tables for X-ray Crystallography*[13]. The atomic number density of the molten CuBr used is 36.3atoms/nm^3 which is taken from the value of its molar volume[14].

Table 1. Numerical values of anomalous dispersion terms $f'(E)$ and $f''(E)$ for Cu and Br used in this work[7].

Energy	$f'_{Cu}(E)$	$f''_{Cu}(E)$	$f'_{Br}(E)$	$f''_{Br}(E)$
8.680 keV (Cu *K* -300eV)	-3.062	0.514	-0.900	1.121
8.955 keV (Cu *K* -25eV)	-5.578	0.485	-0.961	1.061
13.170 keV (Br *K* -300eV)	0.002	2.064	-3.366	0.527
13.445 keV (Br *K* -25eV)	0.040	1.993	-5.815	0.507
17.0 keV	0.255	1.329	-0.481	2.572

3. Partial structural functions

The coherent X-ray intensity profiles of molten CuBr in electron units per atom are shown in Fig.3. These profiles were obtained from the measurements at incident energies of 8.680, 8.955, 13.170 and 13.445 keV, which are 300 and 25eV below the Cu *K* (8.980 keV) and Br *K* (13.470 keV) absorption edges, respectively. The intensity profile measured using the energy of 17.0 keV, which is far from both absorption edges, is also given in this figure. The resultant intensities show remarkable energy dependence and such variations in intensity should be attributed to the change in the anomalous dispersion effects of Cu and Br. It is noted that a small pre-peak denoted by an arrow is also recognized in these profiles. Such pre-peak was observed in other molten copper or silver halides[15)16)]. The energy dependence of this pre-peak intensity at the Cu *K* absorption edge is distinct in comparison with that measured at the Br *K* absorption edge. For this reason, when this correlation distance relevant to the pre-peak is assumed to be the Cu-Cu pairs without any further long distance correlation of Cu, the corresponding scattering intensity may be approximated by $I_{CuCu}(Q) \cong \sin(Qr_{CuCu})/(Qr_{CuCu})$ and the peak position of Q reflects the maximum of the Qr function. On the other hand, an empirical relation between the correlation length r in real space and the peak position Q in an intensity profile, $Qr=2.5\pi$, is suggested in various liquid alloys[3)]. With these facts in mind, the pre-peak position detected in molten CuBr gives the corresponding correlation length of 0.79 nm, so that it is quite likely that a particular density fluctuation of the order of 0.8 nm for Cu is present in molten CuBr.

Figure 4 gives the environmental interference functions $Q\Delta i_{Cu}(Q)$ for Cu and $Q\Delta i_{Br}(Q)$ for Br together with the ordinary interference function of $Qi(Q)$. Figure 5 shows three partial structure factors of molten CuBr calculated directly from the experimental data of Fig. 4 obtained with five different energies by solving the simultaneous linear equation of (6). The results are rather

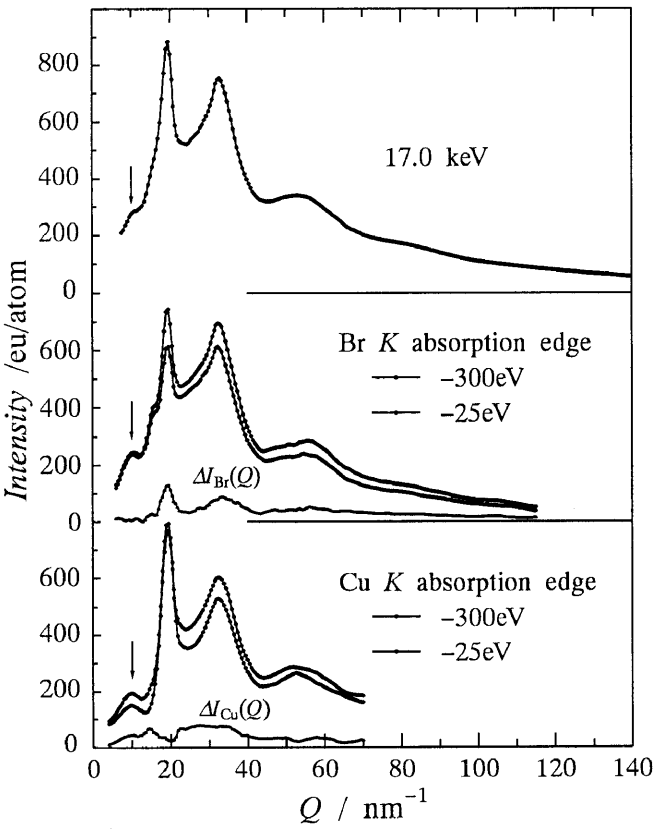

Fig. 3 Coherent X-ray scattering intensity profiles of molten CuBr at 810 K in electron units per atom measured at incident energies of 8.680, 8.955, 13.170, 13.445 and 17.0 keV[12)].

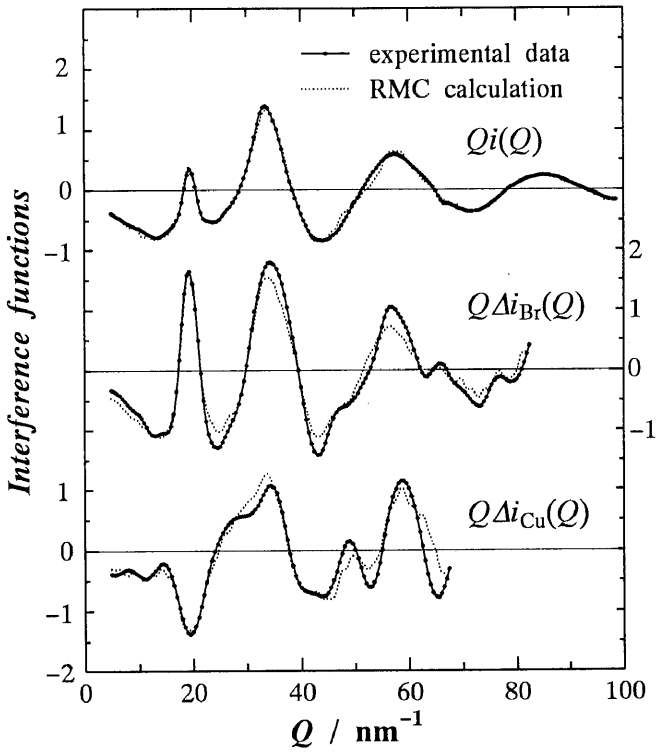

Fig. 4 The ordinary interference function $Qi(Q)$ and the environmental interference functions $Q\ \Delta\ i_{Br}(Q)$ and $Q\ \Delta\ i_{Cu}(Q)$ of molten CuBr. Solid lines correspond to the experimental data. Dotted lines denote values calculated by RMC method.

widely spread in certain positions. Such behavior is known mainly due to the experimental uncertainty such as the relatively small difference between the anomalous dispersion terms at two energies and the unpredictable large fluctuation in numerical solution of eq.(6), when the pivot of matrix is close to zero[17]. Therefore, the present authors are not discouraged from the results of Fig. 5 and rather maintain the view that the variations detected are sizable. Furthermore, we could cite that the profiles of $a_{BrBr}(Q)$ and $a_{CuBr}(Q)$ are very similar to those of simple ionic liquids such as molten alkali halides[18], by observing the first valley of $a_{CuBr}(Q)$ is located at Q value where the principal peak in $a_{BrBr}(Q)$ is situated. In contrast to this observation, the partial structure factor of $a_{CuCu}(Q)$ indicates a structureless profile which is rather similar to the molten CuCl case[5)19]. Several attempts[20)~23] are reported for interpreting such characteristic structural feature of molten CuCl, They are outside of scope of the present work and the definite conclusion is not yet obtained in order to explain the characteristic structure and electronic transport and thermodynamic properties of molten CuCl.

As easily seen in Fig. 5, the numerical solutions of simultaneous linear equations of (6) appear to be ill conditioned in several Q values, producing the large uncertainties, possibly giving some physically unreasonable behavior in the resultant radial distribution functions. At the present time, such small experimental errors cannot always be avoided within the best knowledge of the present authors. The reverse Monte Carlo (hereafter referred as RMC) simulation technique[24] might be one way for reducing this inconvenience. Then, we used the RMC method along the way essentially identical to that described by McGreevy and Pusztai[24] with an initial configuration of 1728 particles, half of them represents Cu^+ ions, the remaining half Br^- ions, in a cubic box of size L=3.624nm. The usual periodic boundary conditions, in which the cube is surrounded by images of itself, are applied and the partial pair distribution functions $g_{\alpha\beta}(r)$'s are calculated. Calculated three interference functions are compared with the experimental results and such comparison is made in the iteration mode until a reasonable convergence is obtained.

The resultant RMC simulation results can reproduce well three independent interference functions of $Q\Delta i_{Cu}(Q)$, $Q\Delta i_{Br}(Q)$ and $Qi(Q)$, as shown in Fig.4. This agreement clearly indicates that the present approach basically works well. The partial structure factors obtained by the RMC simulation technique are given by solid lines in Fig. 5. It should be mentioned that this RMC simulation technique is not a unique mathematical procedure. Nevertheless, the partial structure factors estimated from the present AXS measurements coupled with the RMC simulation technique are considered, in the present authors' view, rather good, and to be at least in a sense of the necessary condition at best, although they might be not the sufficient condition. In addition, all RMC structure factors coincide with the average values of the experimental error bars so as to draw a smooth continuous function.

Figure 6 shows the partial pair distribution functions $g_{\alpha\beta}(r)$ of molten CuBr. The closest Cu-Cu distance is significantly smaller than that for Br-Br, indicating the

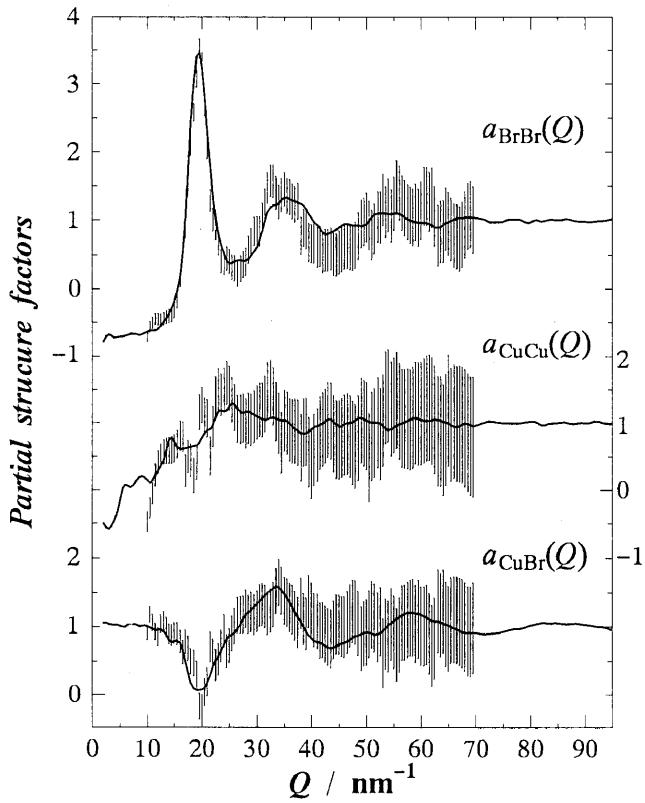

Fig. 5 Three partial structure factors of molten CuBr at 810 K. Solid lines correspond to the values calculated by RMC method.

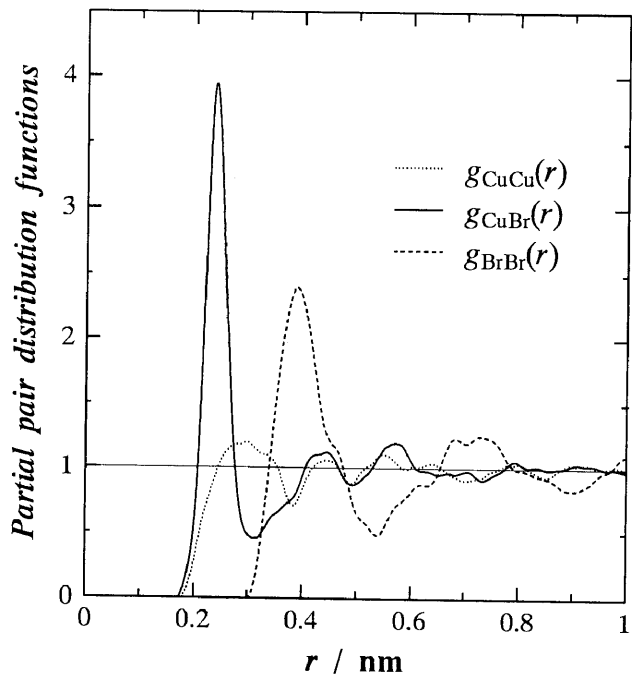

Fig. 6 Three partial pair distribution functions of molten CuBr at 810 K.

like-ion penetration into the first unlike-ion coordination shell. It may be worth mentioning that an attempt was made to replace the Cu-Cu closest distance with the same value of the Br-Br case, but such modification gave gross disagreement between the calculated and the experimental data. The peak positions and the coordination numbers of molten CuBr determined from the present AXS data are found to be consistent with the values obtained by neutron diffraction with isotope substitution[25]. The coordination numbers for Br-Br and Cu-Br pairs are 11.4 at the distance of 0.398nm and 3.1 at the distance of 0.245nm on the average, respectively. These values are rather similar to those for low-temperature phase of γ-CuBr, in which the anions form a fcc lattice, than those for a high-temperature superionic phase of α-CuBr possessing a bcc sub-lattice. It may also be noticed that integration of $r^2 g_{CuCu}(r)$ up to the first minimum in $r^2 g_{CuBr}(r)$ gives 1.2 Cu^+ ions penetrating to the first unlike-ion coordination shell. This characteristic penetration may be interpreted by a decrease in the Coulombic repulsion force interacting between Cu^+ ions due to the reduced charge transfer between unlike ions.

4. Effective pair potentials

The effective pair potentials of the constituents in liquids are widely used for explaining their structure and properties at a microscopic level. Of course, the potential energy of the real molten salts can not be absolutely described by the simple sum of individual pair potentials. However, it is also known to be quite useful to present liquid structure using the "effective" pair potential including many-body effects. In this sense, following the pioneer work of Johnson and March[9] and an advanced method proposed by Reatto, Levesque and Weis[26], there are many attempts to estimate the effective pair potentials of liquids from the experimental structural data, because the experimental structural data are considered to automatically include, more or less, the particular features of liquid of interest. These approaches could be valuable in cases where theoretical estimation of the pair potentials are found to be difficult.

Asymptotic behavior attributed to a long-range Coulomb interaction must be taken into account, when we estimate the effective pair potentials of molten salts. This is known not to be a easy task. This prompts us to estimate the effective pair potentials of molten CuBr from the partial structure factor data determined by the anomalous X-ray scattering method. The resultant pair potentials of molten CuBr are also subject to a comparison with the pair potential proposed by Stafford *et al.*[27]

The procedure for estimating the effective pair potentials of molten salts has already been discussed in detail[28]. Thus, only essential points which are necessary for the present work are given below. The effective pair potential $u_{ab}(r)$ between α and β components can be estimated from measured structural functions using the following modified hypernetted-chain (MHNC) equation[8];

$$u_{\alpha\beta}(r) = k_B T\left[g_{\alpha\beta}(r) - 1 - c_{\alpha\beta}(r) - \ln g_{\alpha\beta}(r) + B_{\alpha\beta}(r)\right]. \quad (7)$$

The pair distribution function $g_{\alpha\beta}(r)$ is known to be connected with the direct correlation function $c_{ab}(r)$ using the Ornstein-Zernike relation as follows;

$$g_{\alpha\beta}(r) - 1 = c_{\alpha\beta}(r) + \sum_{\gamma} n_{\gamma} \int \left[g_{\alpha\gamma}(|\mathbf{r} - \mathbf{r}'|) - 1\right] \cdot c_{\gamma\beta}(r')\mathrm{d}\mathbf{r}' \ , \quad (8)$$

where n_α is number density of the α component. $B_{\alpha\beta}(r)$ is called a bridge function which is a sum of the contribution of all elementary graphs in the cluster expansion. Using measured partial structure factors, both direct correlation functions and pair distribution functions can readily be calculated by the Fourier transformation.

It is difficult to obtain the accurate structure factor data in the very low wave vector region by diffraction experiments. Thus, the results of the MHNC equation using an appropriate model potential was superimposed on the experimental data in such low wave vector region, where the model asymptotic form well satisfies the relation for Fourier transform of the direct correlation functions of $C_{\alpha\beta}(Q)=-4\pi Z_\alpha Z_\beta e^2/(Q^2 k_B T)$ $(Q \rightarrow 0)$. In the present case, we use a model potential proposed by Stafford *et al*[27]. The effective ionic charge is $|Z_\alpha|=0.4828$ for CuBr, which is determined so as to fit a rigid-ion model with the phonon dispersion curves measured by neutron inelastic scattering[29]. The long-wavelength limit of the structure factor described by MHNC equation was adjusted to give a consistent value calculated from the isothermal compressibility and the number density data. The values of density[14] and isothermal compressibility[30] are taken as 0.0181×10^{30} m^{-3} and 1.91×10^{-10} m^2N^{-1} for molten CuBr at 810 K.

At the first predictor stage, we solved eq. (7) with the bridge functions as $B_{\alpha\beta}(r)=0$ and obtained the initial pair potentials $u_{\alpha\beta}(r)$. On the next corrector stage, we carried out the Monte Carlo (MC) simulation with 1728 particles (864 cations and 864 anions), which corresponds to a cell

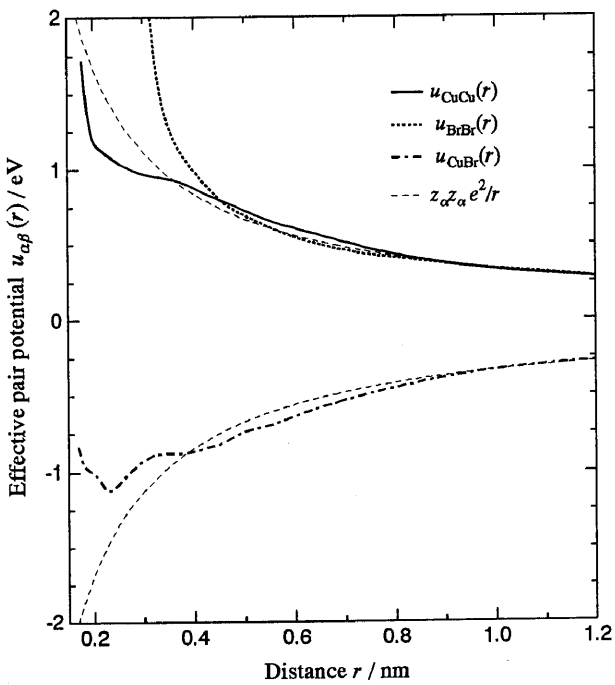

Fig. 7 Three effective pair potentials of molten CuBr at 810 K estimated from the experimental partial structural data. Dotted lines are model potentials proposed by Stafford *et al.*[27]

size of $L^3 = 3.63^3$ nm^3 for liquid CuBr. The long-range Coulomb potential energy was calculated by Ewald method. In the first corrector stage by MC simulation, 10^7 trials were made to realize the equilibrium state. In the second or more iterated process, 2×10^6 trials was found to be sufficient to obtain the equilibrium state. 1500 configurations in the last 1.5×10^6 trials were collected to calculate the pair distribution functions. Eq. (7) is again solved in order to revise the pair potentials. This procedure is repeated until the obtained pair potentials are essentially unchanged. Such process was found to be converged within 10 or 11 times iteration.

Figure 7 shows the effective pair potentials of molten CuBr estimated in this work together with model potentials proposed by Stafford *et al.* [27]. The Cu-Cu pair potential shows the negative deviation from the model potential in the range from 0.2 to 0.35 nm as denoted by the arrow. The deviation from the model potential is also recognized in the potential of Cu-Br pairs in the range from 0.4 to 0.9 nm. These features contrasts to the case of liquid NaCl, in which the pair potentials are well described by the Coulombic and ionic core repulsion forces[28].

In order to facilitate the understanding the structure-potential relationships in molten CuBr, MC simulation was also made using the potentials presently obtained and the model potentials of Stafford *et al.* [27]. The resultant partial structure factors are compared with the experimental partial structure factors in Fig. 8. The following remarks could be drown from these results.

(1) The experimental structure factor of Cu-Cu pairs appears to be well reproduced by the MC simulation using the effective pair potential presently obtained. This includes a particular pre-peak at about Q=10 nm^{-1}. On the contrary, the simulated result using the model potential clearly differs from the experiment. This could be attributed to the marked difference detected in the range of 0.2 ~ 0.35 nm. The present result of the Cu-Cu pair potential suggests more freely movement of Cu ions by making available a lower value at the repulsive core part than the model potential case. As a result, we could obtain very weak Cu-Cu pair correlation.

(2) The present results of the Cu-Br pair potential shows a shallow minimum when compared with the model potential case in the first neighbor region. It is also noticed that there is a negative deviation from the Coulomb potential in the range from 0.4 to 0.9 nm, which is opposite to the case of the Cu-Cu pair potential. The deviation of the Cu-Br pair potential from the Coulombic form is considered to be essential for the understanding of the density fluctuation of Cu ions by keeping the charge neutrality in Coulomb liquids. It would also be noted that a particular feature can be easily seen in the depth of the first valley of the Cu-Br partial structure factor shown in Fig. 8.

(3) The present result of the Br-Br pair potential is, in the authors' view, rather close to the model potential; this contrasts to the Cu-Cu and Cu-Br cases. As a result, fairly good agreement is observed for the partial structure factor simulated using these two potentials, although there are differences in detail.

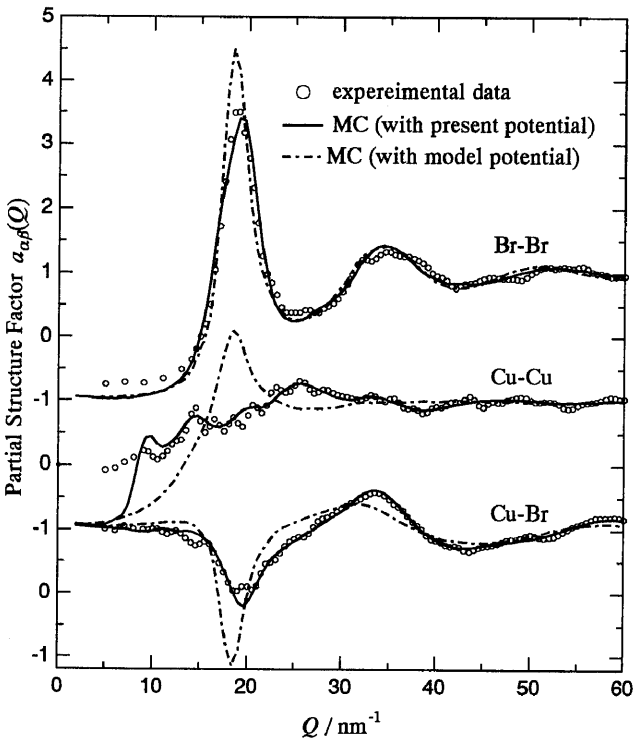

Fig. 8 Partial structure factors of molten CuBr simulated with pair potentials presently obtained (solid line) and model potentials (dotted broken line). The experimental data (circle) are also shown for comparison.

5. Concluding remarks

The present results show good capability of the anomalous X-ray scattering (AXS) measurements for estimating the partial structural functions of liquids again, although the scarcity of absolutely high accuracy for experimental data still prevents us the exact solutions of simultaneous linear equations from the AXS measurements alone. We believe that the reverse Monte Carlo simulation technique is one way to reduce such difficulty by providing information in a sense of the necessary condition at best. The effective pair potentials of molten CuBr were also estimated from the AXS data. From a comparison of the simulated results with the potential in this work and the model potential, the origin of very weak correlation of Cu-Cu pairs in molten CuBr is suggested to arise from the effect of anomalous shielding of the Cu-Cu repulsion force near the first coordination shell. For further discussion about the origin of the characteristic structural features of molten copper halides, additional systematic effort is, of course, required and this includes more accurate determination of the partial structure factor data in the low wave vector region. Nevertheless, it is rather the intention of the present work to indicate that the AXS data enables us a significant step forward for obtaining a direct link between the atomic scale structure and characteristic properties of molten salts. Thus, it would be interesting to extend the AXS measurements to the estimation of the partial structural functions of various molten salts. It may also be noted that the AXS method is the alternative to the isotope substitution of neutron diffraction with the advantage that

all measurements use the same sample.

Acknowledgments

The authors wish to express their gratitude to Prof. M. Nomura, Photon Factory, National Laboratory for High-Energy Physics, for his help on the AXS measurements (Proposal No. 96G100). A part of this work was supported by a Grant-in-Aid for Scientific Research on Priority Area (No.257), from the Ministry of Education, Science and Culture of Japan (No. 07236104) and the New Energy and Industrial Technology Development Organization (NEDO) through the Japan Space Utilization Promotion Center (JSUP) in the program " Technology for Production of High Quality Crystal" of the Ministry of International Trade and Industry (MITI).

References

1) G.H.A.Cole: *An Introduction to the Statistical Theory of Classical Simple Fluids*, (Pergamon Press, New York, 1967).
2) T.E.Faber : An Introduction to the Theory of Liquid Metals, (Cambridge University Press, Cambridge, 1972).
3) Y. Waseda: *The Structure of Non-Crystalline Materials*, (McGraw-Hill, New York, 1980), p.60.
4) J. E. Enderby, D. M. North and P. A. Egelstaff: Phil. Mag. **14** (1966) 961.
5) D. I. Page and I. Mika: J. Phys. **C4** (1971) 3034.
6) R.W.James: *Optical Principles of the Diffraction of X-rays*, (G.Bell and Sons Ltd., London, 1948).
7) Y. Waseda: *Novel Application of Anomalous X-ray Scattering for Structural Characterization of Disordered Materials*,(Springer-Verlag, New York, 1984).
8)Y.Rosenfeld and N.W.Ashcroft: Phys. Rev., **A20** (1979) 1208.
9) M. D. Johnson and M. H. March: Phys. Lett. **3** (1963) 313.
10) T. G. Ramesh and S. Ramaseshan: J. Phys. **C4** (1971) 3029.
11) D. T. Cormer and D. A. Liberman: J. Chem. Phys. **53** (1970), 1891
12) M.Saito, C.Y.Park, K.Omote, K.Sugiyama and Y. Waseda: J.Phys. Soc. Jpn, **66** (1997), (in press).
13) J. A. Ibers and W. C. Hamilton ed.: *International Tables for X-ray Crystallography vol. IV*, (Birmingham, Kynoch, 1974).
14) M. Inui, S. Takeda and T.Uechi: J. Phys. Soc. Jpn. **60** (1991) 3190.
15) Y. Shirakawa, M. Saito, S. Tamaki, M. Inui and S. Takeda: J. Phys. Soc. Jpn. **60** (1991) 2678.
16) M. Inui, S. Takeda, Y. Shirakawa, S. Tamaki, Y. Waseda and Y. Yamaguchi: J. Phys. Soc. Jpn. **60** (1991) 3025.
17) R. G. Stantson: *Numerical Methods for Science and Engineering*, (Prentice-Hall, New York, 1961), Chaps. 7 and 8.
18) S.Biggins and J.E.Enderby: J.Phys. C: Solid State Phys., **15** (1982)L305.
19) S. Eisenberg, S. F. Jal, J. Dupuy, P. Chieux and W. Knoll: Phil. Mag. A**46** (1982) 195.
20) J. M. Powels: J. Phys. **C8** (1975) 895.
21) M. J. Gillan: J. Phys. **C9** (1976) 2261.
22) J. Trullas, A. Giro, J. A. Padro and M. Silbert: Physica, **A 171** (1991) 384.
23) M. C. Abrano, C. Caccamo, G. Pizzimenti, M. Parrinello and M. P. Tosi, J. Phys. **C9** (1976) L593.
24) R. L. McGreevy and L. Pusztai: Mol. Simulation **1** (1988) 359.
25) D. A. Allen and R. A. Howe: J. Phys.: Condens. Matter **4** (1992) 6029.
26) L. Reatto, D. Levesqure and J. J. Weis: Phys. Rev. **A 33** (1986) 3451.
27) A. J. Stafford, M. Silbert, J. Trullas and A. Giro : J. Phys. : Cond. Matter **2** (1990) 6631.
28) K.Omote and Y.Waseda: J. Phys. Soc. Jpn. **66** (1997), (in press).
29) B. Prevot, C. Carabatos and C. Schwab : Solid. State Comm. **13** (1973) 1725.
30) S. Takeda, Y. Shirakawa, K. Takesawa, S. Harada and S. Tamaki : J. Phys. Soc. Jpn. **58** (1989) 4007.